*Journal of Advanced Ceramics*
2018, **7**(2): 169–177
https://doi.org/10.1007/s40145-018-0268-2
ISSN 2226-4108
CN 10-1154/TQ

**Research Article**

# KD-S $SiC_f$/SiC composites with BN interface fabricated by polymer infiltration and pyrolysis process

Honglei WANG[a,b], Shitao GAO[b], Shuming PENG[a], Xingui ZHOU[b,*], Haibin ZHANG[a], Xiaosong ZHOU[a], Bin LI[b,*]

[a]*Innovation Research Team for Advanced Ceramics*, *Institute of Nuclear Physics and Chemistry*, *China Academy of Engineering Physics*, *Mianyang*, *Sicuan 621900*, *China*
[b]*Science and Technology on Advanced Ceramic Fibers and Composites Laboratory*, *National University of Defense Technology*, *Changsha*, *Hunan 410073*, *China*

Received: December 8, 2017; Accepted: March 13, 2018
© The Author(s) 2018. This article is published with open access at Springerlink.com

**Abstract:** Continuous silicon carbide fiber reinforced silicon carbide matrix ($SiC_f$/SiC) composites are attractive candidate materials for aerospace engine system and nuclear reactor system. In this paper, $SiC_f$/SiC composites were fabricated by polymer infiltration and pyrolysis (PIP) process using KD-S fiber as the reinforcement and the LPVCS as the precursor, while the BN interface layer was introduced by chemical vapor deposition (CVD) process using borazine as the single precursor. The effect of the BN interface layer on the structure and properties of the $SiC_f$/SiC composites was comprehensively investigated. The results showed that the BN interface layer significantly improved the mechanical properties of the KD-S $SiC_f$/SiC composites. The flexure strength and fracture toughness of the KD-S $SiC_f$/SiC composites were evidently improved from 314±44.8 to 818±39.6 MPa and 8.6±0.5 to 23.0±2.2 MPa·$m^{1/2}$, respectively. The observation of TEM analysis displayed a turbostratic structure of the CVD-BN interface layer that facilitated the improvement of the fracture toughness of the $SiC_f$/SiC composites. The thermal conductivity of KD-S $SiC_f$/SiC composites with BN interface layer was lower than that of KD-S $SiC_f$/SiC composites without BN interface layer, which could be attributed to the relative low thermal conductivity of BN interface layer with low crystallinity.

**Keywords:** silicon carbide (SiC); composites; interface layer; polymer infiltration and pyrolysis (PIP); boron nitride (BN)

## 1 Introduction

Silicon carbide (SiC) is a promising candidate for many high-temperature applications such as aerospace engine system, nuclear fusion and fission reactor system, catalyst carrier, and semiconductor element, owing to its excellent properties including high hardness, good oxidation resistance, high thermal conductivity, outstanding stability in severe environment, and low induced radioactivation under neutron irradiation [1–3]. However, the brittle character of the monolithic SiC hampers its direct utilization as high-temperature structure materials in aerospace and nuclear systems.

In order to get over the brittle character of monolithic

*Corresponding authors.
E-mail: X. Zhou, zhouxinguilmy@163.com;
B. Li, libin@nudt.edu.cn

SiC, the continuous SiC fiber is introduced into monolithic SiC as the reinforcement, which can be defined as continuous SiC fiber reinforced SiC matrix ($SiC_f$/SiC) composites. $SiC_f$/SiC composites have the advantages of low density, high specific strength/modulus, thermal-shock resistance, and non-catastrophic mode of failure. Meanwhile, $SiC_f$/SiC composites also possess most of the inherent character of monolithic SiC [4–8].

Up to date, several methods have been applied to fabricate $SiC_f$/SiC composites, such as chemical vapor infiltration (CVI) [9–11], polymer infiltration and pyrolysis (PIP) [12–14], melt infiltration (MI) [15–19], and nano-infiltration and transient eutectoid (NITE) [20–22]. Compared to other methods, the PIP process has its advantages in fabrication of large-scale components with complex shape, composition design, and microstructural control. However, the conventional PIP process using polycarbosilane (PCS) as precursor has many defects including high porosity, low densification efficiency, long fabrication period, and high fabrication cost. In order to overcome these problems, new precursor has been developed to fabricate SiC matrix in PIP process, such as allylhydridopolycarbosilane (AHPCS) and LPVCS [13,14,23,24].

Moreover, the kinds of SiC fibers remarkably affect the preparation and properties of the $SiC_f$/SiC composites. So far, three generations of SiC fibers have been developed by optimizing their composition and microstructure. The thermal resistance of the third generation of SiC fibers (including Hi-Nicalon-S, Sylramic and Tyranno SA) has achieved 1800 ℃ due to their low oxygen content and high crystallinity [25,26]. Recently, the National University of Defense Technology (NUDT) in China has developed the third generation of SiC fibers, which was named as KD-S SiC fibers. The studies on the $SiC_f$/SiC composites using Hi-Nicalon-S, Sylramic and Tyranno SA as reinforcement have been widely reported [27–31]. However, the research on the KD-S SiC fiber using as reinforcement in the $SiC_f$/SiC composites has been barely mentioned.

Additionally, the interface layer, which connects the fiber and matrix, plays an important role in determining the properties of the composites. The interface layer not only prevents damage of the fiber during the fabrication process, but also transfers the load from the matrix to the fiber [32]. The pyrolytic carbon (PyC) and hexagonal boron nitride (h-BN) are considered as the effective interface layers for the $SiC_f$/SiC composites thanks to their layered microstructure. However, the PyC interface layer is easily oxidized in oxidizing atmosphere even at lower temperature, resulting in the degradation of the mechanical properties of the $SiC_f$/SiC composites. The BN interface layer will effectively improve the oxidation resistance of the $SiC_f$/SiC composites, because BN can be oxidized into vitreous $B_2O_3$ at ~800 ℃. The self-healing feature of the vitreous $B_2O_3$ hampers further oxidation of $SiC_f$/SiC composites [33]. Several methods have been developed for fabrication of BN interface layer such as chemical vapor deposition (CVD) and dip-coating. However, the mostly applied method is CVD process due to the poorer uniform structure and composition purity of BN interface layer fabricated by dip-coating process [34–37]. Conventional CVD process for fabrication of BN adopts $BX_3$–$NH_3$ (X can be F, Cl, or Br) as growth precursor. However, the byproducts such as HF and HCl cause the degradation of SiC fiber because of their strong corrosion. Many born-organics including $H_3BN(C_2H_5)_3$, $H_3BNH(C_3H_3)_2$, and $B_3N_3(CH_3)_9$ also can be utilized as precursors to deposit BN interface layer. However, C and O impurities could be easily introduced into the CVD-BN interface layer. Recently, borazine ($B_3N_3H_6$) has been used as precursor for fabricating BN coating by Li *et al.* [38] and Gao *et al.* [39]. The borazine is a promising single precursor for CVD-BN due to its boron–nitrogen stoichiometry without impurity element. However, the BN interface layer fabricated by CVD process using borazine as precursor has not been reported in the studies on the $SiC_f$/SiC composites.

In this work, in order to investigate the effect of the BN interface layer on the structure and properties of the $SiC_f$/SiC composites, BN interface layer was fabricated by CVD process using borazine as the single precursor. Additionally, KD-S fiber was adopted as the reinforcement, and LPVCS was utilized as the polymer precursor for the fabrication of $SiC_f$/SiC composites.

## 2 Experimental procedure

The KD-S SiC fibers (reinforcement) were provided by NUDT. General properties of the KD-S fibers are listed in Table 1. Firstly, the three-dimensional four-directional (3D4d) KD-S SiC fiber fabrics were braided by three-dimensional four-step braiding technique. The

**Table 1 Properties of KD-S SiC fiber**

| SiC fiber | C/Si atomic ratio | Oxygen content (wt%) | Bulk density ($g/cm^3$) | Diameter (μm) | Tensile strength (GPa) | Tensile modulus (GPa) |
|---|---|---|---|---|---|---|
| KD-S | 1.05 | 1.0 | 2.85 | 11 | 2.6 | 320 |

fiber volume fraction was approximately 50% (Key Laboratory of Advanced Textile Composite Materials, Tianjin Polytechnic University, Tianjin, China).

Then, BN interface layer was introduced into the SiC fiber fabrics by CVD at 1100 ℃ for 2 h in a vertical hot-wall reaction system. Borazine was adopted as the single source precursor of BN interface in CVD process. The borazine adopted in this paper was synthesized and purified according to Li *et al.*'s previous work [39]. The liquid precursor borazine was contained in a bubbler, which was maintained at 0 ℃ during the CVD process. The borazine was delivered from the bubbler to the reaction furnace using nitrogen ($N_2$, 99.999%) as the carrier and dilute gas. The flow rate of gas mixture (borazine and $N_2$) was maintained at 800 sccm dosed controlled by gas mass flow meter. The total pressure of CVD process was kept at 250 Pa using automatic pressure controller. Finally, LPVCS (provided by NUDT) with a viscosity of 20 mPa·s at room temperature was used as the SiC matrix precursor, which was the mixture of 2,4,6,8-Tetraviny-2,4,6,8-Tetramethylcyclotetrasiloxane(V4) and liquidpolycarbosilane (LPCS) with a weight ratio of 0.6:1. The BN coated KD-S SiC fiber fabrics were impregnated with LPVCS via vacuum infiltration for 24 h, and a thermal pressure-assisted (3 MPa) curing procedure was applied after the first impregnation with 1 ℃/min up to 300 ℃. Then, the fabrics were heated up to 1200 ℃ with a heating rate of 10 ℃/min in an inert argon atmosphere for 30 min. Subsequently, the repetition of impregnation and pyrolysis procedure was finished until the weight increase of the composites was less than 1%. The process flow is shown in Fig. 1.

The morphologies of the KD-S SiC fiber with BN interface layer were observed using field emission scanning electron microscopy (FESEM, HITACHI UHR SU8010, Japan). The chemical bonds of the KD-S SiC fiber with and without BN interface layer were analyzed by Fourier transform infrared spectroscopy (FTIR, Thermo Fisher Scientific Nicolet 6700, USA). The KD-S SiC fibers with and without BN interface layer were ground into powder, and then compacted into pellets with KBr for the FTIR analysis.

The single filament tensile strength and modulus of the KD-S SiC fiber with and without BN interface layer were measured using a single filament strength electronic tester (TestometrixMicro350, UK). The test span was 25 mm and the test speed was 5 $mm \cdot min^{-1}$ according to ASTMD 3379-75. The sample quantity of the single filament tensile strength test was more than 50.

The density and open porosity of the KD-S $SiC_f$/SiC composites were measured by Archimedes principle using kerosene as medium. The flexural strength of the KD-S $SiC_f$/SiC composites was measured by three-point bending method at room temperature. The dimension of the test sample was 2.5 mm ($H$) × 3.5 mm ($B$) × 40 mm ($L$). The span length was 30 mm, and the crosshead speed was 0.5 mm/min. The fracture toughness of the KD-S $SiC_f$/SiC composites was measured by single-edged notch beam method at room temperature. The dimension of the test sample was 5 mm ($H$) × 2.5 mm ($B$) × 40mm ($L$). The span length was 30 mm, the notch depth was 2.5 mm, and the crosshead speed was 0.05 mm/min. Both tests were performed on a universal testing machine (C45.105, MTS, USA). The numbers of samples for the three-point bending and single-edged notch beam tests were 5 and 5, respectively. The fracture surface and microstructure of the KD-S $SiC_f$/SiC composites were examined using FESEM. The thermal diffusivity, $\alpha$, was measured using flash method at room temperature. The size of specimens for thermal diffusivity was 12.7 mm in diameter and 2.5 mm in thickness. The specific heat, $C_p$, was tested

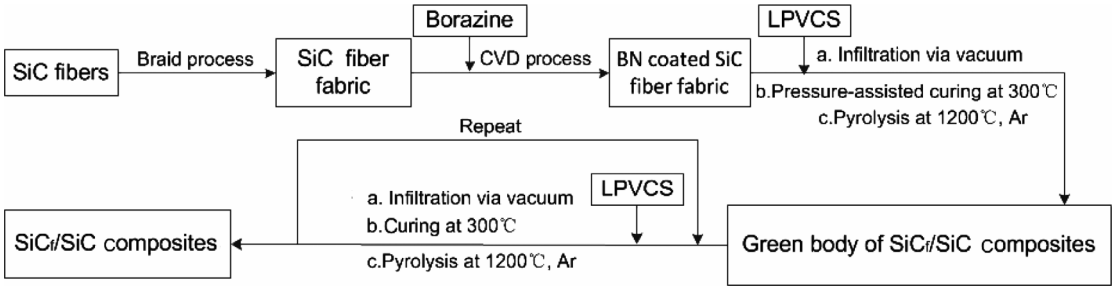


**Fig. 1** Flow chart of the fabrication process of the KD-S $SiC_f$/SiC composites.

by means of differential scanning calorimetry, using single-crystal alumina as a reference material. The thermal conductivity, $\lambda$, was calculated by the formula $\lambda = \rho C_p \alpha$. The microstructure of the KD-S $SiC_f$/SiC composites with BN interface layer was examined using high resolution transmission electron microscopy (HRTEM, JEOL JEM 2100). The TEM specimens were prepared utilizing the focused ion beam (FIB) method by FEI Helios Nanolab 600 Dual Beam FIB/SEM.

## 3 Results and discussion

The morphologies of the BN interface layer fabricated by CVD process using borazine as the single precursor are shown in Fig. 2. As can be seen, the BN interface layer deposited on surface of the KD-S SiC fiber is uniform and continuous, and the thickness is about 400 nm. It also can be seen that the BN interface layer surrounds tightly on the surface of the KD-S SiC fiber. It indicates that the BN interface layer fabricated by CVD process has a good thermal matching with the KD-S SiC fiber. Compared to the BN coating fabricated by dip-coating process, the surface of BN coating on the KD-S SiC fiber reveals that the BN interface layer prepared by CVD process is more smooth and dense.

FTIR was utilized to confirm the phase composition of BN interface layer deposited on the KD-S SiC fiber (see Fig. 3). The absorption peaks around 1080, 830, and 460 $cm^{-1}$ are detected in both as-received SiC fiber and BN-coated SiC fiber, attributed to Si–O–Si stretching vibration, Si–C stretching vibration, and Si–O bending vibration, respectively. The observation of characteristic absorption bands for Si–O–Si and Si–O implies that the KD-S SiC fiber has a certain amount of oxygen, which exists in the form of Si–C–O phase within the KD-S SiC fiber. The peaks around 1380 and 810 $cm^{-1}$ are detected for the KD-S SiC fiber deposited with BN interface layer, which are attributed to B–N in-plane stretching vibrations and B–N–B out-of-plane bending vibrations, respectively [39]. It indicates that BN interface layer prepared by CVD process using borazine as the single precursor is typical h-BN. However, compared to the well-crystallized h-BN, the absorption band around 1380 and 810 $cm^{-1}$ is evidently broad. It means that the BN interface layer deposited at 1100 ℃ is partially ordered h-BN, which is confirmed by HRTEM observation in the following section.

The single filament mechanical properties of KD-S SiC fiber with and without BN interface layer are listed in Table 2. The values indicate that the as-received KD-S SiC fiber has a tensile strength of 2.61±0.77 GPa and tensile modulus of 284±35 GPa, which is consistent with the values listed in Table 1. After the KD-S SiC fiber is deposited with BN interface layer by CVD process, the tensile strength of the KD-S SiC fiber slightly decreases, while the tensile modulus slightly increases. It means that the CVD process has little effect on the single filament mechanical properties of KD-S SiC fiber due to its high thermal stability.

The properties of KD-S $SiC_f$/SiC composites with and without BN interface layer are shown in Table 3. The density and open porosity of the KD-S $SiC_f$/SiC composites with and without BN interface layer are close to each other (the density and open porosity of the composites are approximately 2.33 $g/cm^3$ and 6%, respectively). The open porosity is significantly lower

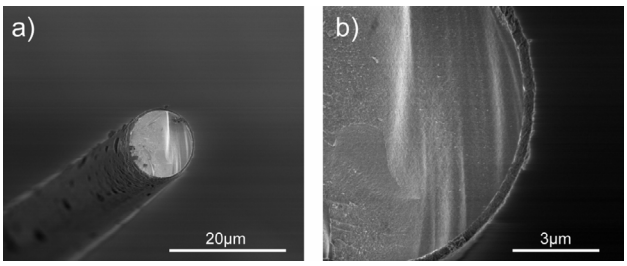


**Fig. 2** SEM images of KD-S SiC fiber with BN interface layer.

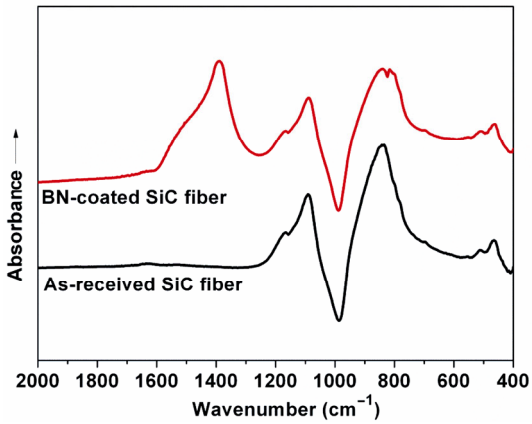


**Fig. 3** FTIR spectra of KD-S SiC fiber with and without BN interface layer.

**Table 2 Single filament mechanical properties of KD-S SiC fiber**

| Fiber | Tensile strength (GPa) | Tensile modulus (GPa) |
|---|---|---|
| As-received | 2.61±0.77 | 284±35 |
| BN interface | 2.38±0.44 | 288±17 |

**Table 3 Properties of the KD-S SiCf/SiC composites with and without BN interface layer at room temperature**

| Interface layer | Density (g/cm$^3$) | Open porosity (%) | Flexural strength (MPa) | Elastic modulus (GPa) | Fracture toughness (MPa·m$^{1/2}$) | Thermal conductivity (W·m$^{-1}$·K$^{-1}$) |
|---|---|---|---|---|---|---|
| Without BN | 2.34 | 6.1 | 314±44.8 | 145±6.6 | 8.6±0.5 | 3.06 |
| With BN | 2.33 | 5.8 | 818±39.6 | 137±14.1 | 23.0±2.2 | 2.34 |

than that of the $SiC_f$/SiC composites fabricated by PIP process using PCS as the polymer precursor [40]. The porosity of the $SiC_f$/SiC composites is mainly caused by the gas evolution and volume shrinkage during the pyrolysis of the polymer precursor. Compared with the PCS, the open porosity of the $SiC_f$/SiC composites fabricated with LPVCS as the polymer precursor is relatively low, due to the superior densification efficiency of the LPVCS. Moreover, the preparation period of PIP process is remarkably shortened using the LPVCS as precursor, resulted from the LPVCS with low viscosity and high ceramic yield.

As shown in Table 3, the KD-S $SiC_f$/SiC composites with BN interface layer exhibit better mechanical properties comparing to the KD-S $SiC_f$/SiC composites without BN interface layer. The flexure strength and fracture toughness of the KD-S $SiC_f$/SiC composites are evidently improved from 314±44.8 to 818±39.6 MPa and 8.6±0.5 to 23.0±2.2 MPa·m$^{1/2}$ respectively, owing to the introduction of BN interface layer. It indicates that the BN interface layer will weaken the fiber–matrix interface bonding, which can prevent the cracks in the matrix propagating to the SiC fiber and damaging the SiC fiber. However, the elasticity modulus of KD-S $SiC_f$/SiC composites with BN interface layer is close to that of KD-S $SiC_f$/SiC composites without BN interface layer, which means that the BN interface layer has little effect on the elasticity modulus of KD-S $SiC_f$/SiC composites.

Table 3 also shows that the thermal conductivity of KD-S $SiC_f$/SiC composites with BN interface layer is lower than that of KD-S $SiC_f$/SiC composites without BN interface layer. It indicates that the BN interface layer hinders the transmission of thermal energy from matrix to fiber, which is due to the low thermal conductivity of BN interface layer with poor crystallization.

Figure 4 shows the typical load–displacement curves of KD-S $SiC_f$/SiC composites with and without BN interface during the three-point bending test. According to Fig. 4, the load on the KD-S $SiC_f$/SiC composites without BN interface decreases sharply as reaching the peak value, which exhibits a catastrophic and brittle mode. It is attributed to the strong fiber–matrix interface bonding, which results in loosing toughening function of the SiC fiber for $SiC_f$/SiC composites because the SiC fibers are clipped by the cracks propagated from the SiC matrix. However, the load–displacement curve of the KD-S $SiC_f$/SiC composites with BN interface exhibits a standard toughened fracture behavior, and fails non-catastrophically. After the load on the KD-S $SiC_f$/SiC composites with BN interface reaches the peak value, the load decreases in a step development tendency as the displacement increases.

Figure 5 shows the fracture morphologies of the KD-S $SiC_f$/SiC composites with and without BN interface layer after bending test. As shown in Figs. 5(a) and 5(b), the fracture surface of the KD-S $SiC_f$/SiC composites without BN interface layer is very flat, and no pulled-out fibers can be observed. It indicates that the KD-S $SiC_f$/SiC composites without BN interface layer have a strong interfacial bonding between the SiC fibers and SiC matrix. This can be attributed to the rough surface characteristics of as-received KD-S SiC fibers, which results in the strong physical interfacial bonding with PIP SiC matrix due to the mechanical bond in interfacial region. On the other hand, for the SiC fibers without interface layer, the strong interfacial bonding between fibers and matrix is caused by the diffusion reaction between the SiC fibers and LPVCS during the process of PIP SiC matrix. The strong interfacial bonding prevents the cracks to deflect as the matrix cracks propagate to the interfacial region between fibers and matrix, which remarkably reduces the fracture absorbing energy of $SiC_f$/SiC composites. This is consistent with the low fracture toughness of the KD-S $SiC_f$/SiC composites without BN interface layer, confirmed by the load–displacement curve during the three-point bending test (see Fig. 4).

Furthermore, SiC fibers without interface layer may be damaged by the reaction, which leads to the reduction of SiC fiber strength. In general, the strength of interfacial bond and fiber mainly determines the mechanical performance of the continuous fiber reinforced ceramic matrix composites (CMCs). Compared to the KD-S $SiC_f$/SiC composites with BN interface layer,

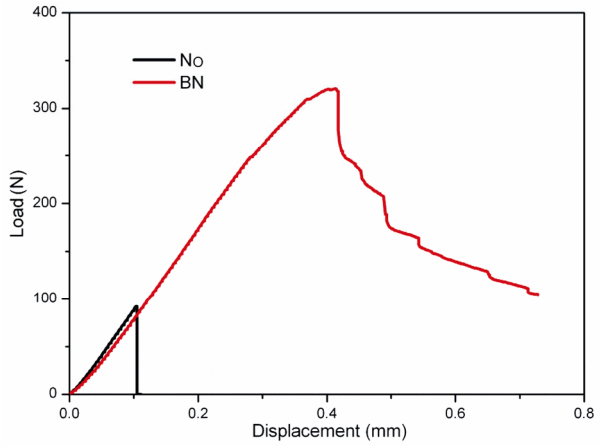


**Fig. 4** Load–displacement curves of the KD-S $SiC_f$/SiC composites with and without BN interface layer.

the KD-S $SiC_f$/SiC composites without BN interface layer show lower mechanical performance, which is attributed to the failure of fiber reinforced mechanism due to the strong interfacial bonding and low fiber strength.

Moreover, it can be seen that a small number of pores with different sizes present in the KD-S $SiC_f$/SiC composites without BN interface layer (Fig. 5(a)). This is due to the gas release and volume shrinkage during the pyrolysis process of the LPVCS. These pores can become the fracture source when the $SiC_f$/SiC composites bearing external load and cracks are generated in the matrix. In order to improve the mechanical properties of the PIP $SiC_f$/SiC composites, the pores in the SiC matrix must be reduced to minimum.

In contrast, the fracture surface of the KD-S $SiC_f$/SiC composites with BN interface layer is relatively uneven and shows obvious fiber pull-out (Figs. 4(c) and 4(d)). Moreover, the pull-out fibers have a long pull-out length, which indicates that the SiC fibers have high strength retention due to the protective effect of BN interface layer during the PIP process. It also indicates that the BN interface layer weakens the interfacial bonding between fibers and matrix, demonstrated by the observation of pull-out fibers covered with a certain amount of BN interface layer (Fig. 5(d)). The BN interface layer leads to a proper bonding strength between fibers and matrix, which results in the pseudo-ductile fracture mechanism of the $SiC_f$/SiC composites through crack deflecting and branching behavior.

Figure 6 shows the TEM images and selected-area electron diffraction (SAED) patterns for each constituent of the KD-S $SiC_f$/SiC composites with BN interface layer. The bright field TEM image taken on the cross-sectional specimen is presented in Fig. 6(a). The darker and brighter grey regions are SiC fiber, SiC matrix, and BN interface layer, respectively. It can be seen that the surface of SiC fiber is covered with uniform BN interface layer with a thickness of ~400 nm, which is consistent with the observation in Fig. 2. In addition, the BN interface layer is well bonded to the SiC fiber. It further indicates that the BN interface layer has similar thermal expansivity with the KD-S SiC fiber.

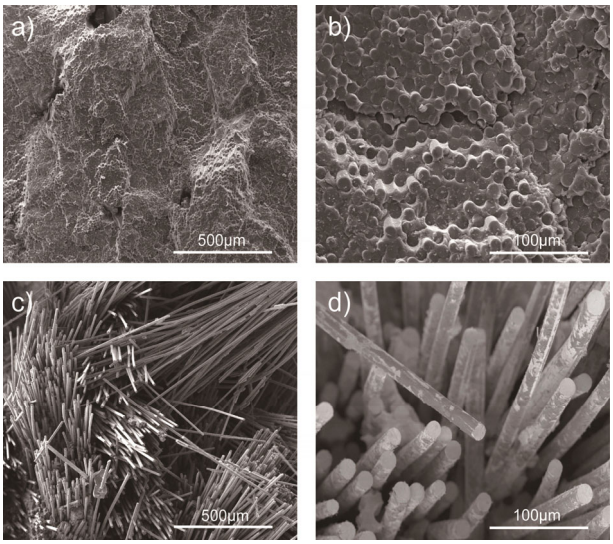


**Fig. 5** Fracture morphologies of the KD-S $SiC_f$/SiC composites (a, b) without and (c, d) with BN interface layer.

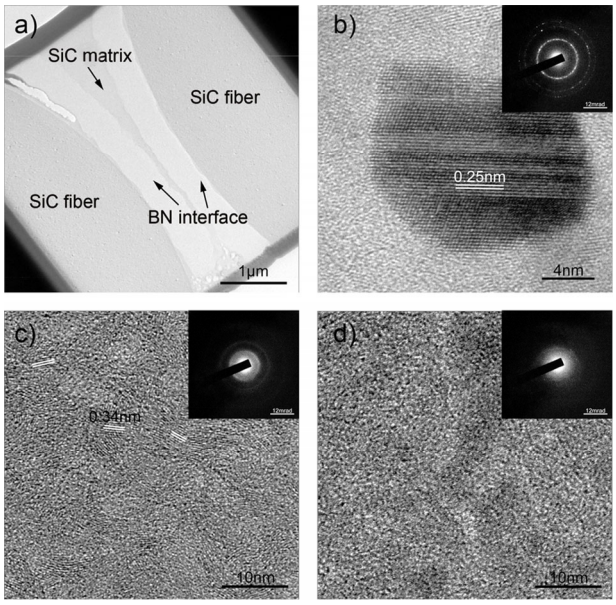


**Fig. 6** TEM images and SAED patterns for each constituent of the KD-S $SiC_f$/SiC composites with BN interface layer: (a) bright field TEM image taken on the cross-sectional specimen, (b) SiC fiber, (c) BN interface, and (d) SiC matrix.

However, there is a gap appearing near the upper left corner of Fig. 6(a), which may be caused by peeling of the BN interface layer during the FIB preparation process of TEM sample. As shown in Fig. 6(b), clear diffraction spots and rings are observed in the SAED pattern, and the diffraction rings correspond to the (111), (220), and (311) planes of the β-SiC phase from the inner to outer part. The observation indicates that the KD-S SiC fiber has a polycrystalline structure. Moreover, Fig. 6(b) shows that the β-SiC of the KD-S SiC fiber has twinning growth. And the distance between lattice planes is measured to be 0.25 nm, which is indexed as the (111) plane of the β-SiC. Also, it can be found that the grain size of β-SiC can reach 16 nm. It confirms that the degree of crystallization of the KD-S SiC fiber is higher than that of KD-I and KD-II SiC fibers [14,41]. Figure 6(c) shows the HRTEM image and SAED pattern of the BN interface layer. The textured BN shows a random rotation in the amorphous region, which is identified as the h-BN nanocrystal with a (002) lattice space of 0.34 nm. This result indicates that the structure of the BN interface layer is turbostratic, which means that the crystallization degree of the BN interface layer is lower. The observation is confirmed by the SAED pattern of the BN interface layer. The poor crystallinity of the BN interface layer will significantly affect the phonon free path and hinder the phonon scattering [42]. So the KD-S $SiC_f$/SiC composites with BN interface layer have shown lower thermal conductivity (Table 2). Additionally, the layered structure of textured BN enables BN interface layer with the required mechanical performance of interface in CMCs. This is because the debonding energy of the layer structure is low, which facilitates the deflection and divarication of cracks generated from the matrix [38]. Therefore, the BN interface layer with layered structure improves the fracture toughness of the $SiC_f$/SiC composites. As shown in Fig. 6(d), the HRTEM image of the SiC matrix indicates that the SiC matrix fabricated at 1200 ℃ possesses typical amorphous structure. And the SAED pattern also exhibits diffuse halos, which demonstrates that the SiC matrix has poor crystallinity.

## 4 Conclusions

The CVD-BN interface layer deposited on surface of the KD-S SiC fiber owned a uniform and continuous structure. The tensile strength of the KD-S SiC fiber slightly decreased and the tensile modulus slightly increased, as the KD-S SiC fiber was deposited with BN interface layer by CVD process.

The KD-S $SiC_f$/SiC composites with and without BN interface layer had similar density and open porosity values (approximately 2.33 g/cm$^3$ and 6%, respectively). The open porosity was lower than that of $SiC_f$/SiC composites prepared by PIP process using PCS as the precursor. LPVCS has higher densification efficiency.

The flexure strength and fracture toughness the KD-S $SiC_f$/SiC composites were evidently improved from 314±44.8 to 818±39.6 MPa and 8.6±0.5 to 23.0± 2.2 MPa·m$^{1/2}$, respectively. The BN interface layer significantly improved the mechanical properties of the KD-S $SiC_f$/SiC composites. However, the thermal conductivity of KD-S $SiC_f$/SiC composites with BN interface layer was lower than that of KD-S $SiC_f$/SiC composites without BN interface layer, which can be attributed to the low thermal conductivity of BN interface layer with poor crystallinity.

The KD-S SiC fiber had a typical polycrystalline structure, and the SiC matrix fabricated by PIP process at 1200 ℃ showed amorphous structure. The turbostratic structure of BN interface layer facilitated the improvement of the fracture toughness of the $SiC_f$/SiC composites.

### Acknowledgements

This work was supported by the National Natural Science Foundation of China with Grant Nos. 51502343 and 91426304.

### References

[1] Madar R. Materials science: Silicon carbide in contention. *Nature* 2004, **430**: 974–975.

[2] Zhao S, Yang Z, Zhou X. Microstructure and mechanical properties of compact SiC/SiC composite fabricated with an infiltrative liquid precursor. *J Am Ceram Soc* 2015, **98**: 1332–1337.

[3] Nozawa T, Hinoki T, Snead LL, *et al*. Neutron irradiation effects on high-crystallinity and near-stoichiometry SiC fibers and their composoites. *J Nucl Mater* 2004, **329–333**: 544–548.

[4] Zhao S, Yang Z, Zhou X, *et al*. Fabrication and characterization of in-situ grown carbon nanotubes reinforced SiC/SiC composite. *Ceram Int* 2016, **42**: 9264–9269.

[5] Katoh Y, Snead LL, Henager Jr. CH, *et al*. Current status

and recent research achievements in SiC/SiC composites. *J Nucl Mater* 2014, **455**: 387–397.

[6] Nozawa T, Hinoki T, Hasegawa A, *et al*. Recent advances and issues in development of silicon carbide composites for fusion applications. *J Nucl Mater* 2009, **386–388**: 622–627.

[7] Snead LL, Nozawa T, Ferraris M, *et al*. Silicon carbide composites as fusion power reactor structural materials. *J Nucl Mater* 2011, **417**: 330–339.

[8] Zhou X-G, Wang H-L, Zhao S. Progress of $SiC_f$/SiC composites for nuclear application. *Adv Ceram* 2016, **37**: 151–167. (in Chinese)

[9] Xu Y, Cheng L, Zhang L, *et al*. High performance 3D textile Hi-Nicalon SiC/SiC composites by chemical vapor infiltration. *Ceram Int* 2001, **27**: 565–570.

[10] Udayakumar A, Sri Ganesh A, Raja S, *et al*. Effect of intermediate heat treatment on mechanical properties of $SiC_f$/SiC composites with BN interphase prepared by ICVI. *J Eur Ceram Soc* 2011, **31**: 1145–1153.

[11] Yang W, Kohyama A, Noda T, *et al*. Interfacial characterization of CVI-SiC/SiC composites. *J Nucl Mater* 2002, **307–311**: 1088–1092.

[12] Zhao S, Zhou X, Yu J. Effect of heat treatment on the mechanical properties of PIP-SiC/SiC composites fabricated with a consolidation process. *Ceram Int* 2014, **40**: 3879–3885.

[13] Kohyama A, Kotani M, Katoh Y, *et al*. High-performance SiC/SiC composites by improved PIP processing with new precursor polymers. *J Nucl Mater* 2000, **283–287**: 565–569.

[14] Luo Z, Zhou X, Yu J. Mechanical properties of SiC/SiC composites by PIP process with a new precursor at elevated temperature. *Mat Sci Eng A* 2014, **607**: 155–161.

[15] Morscher GN, John R, Zawada L, *et al*. Creep in vacuum of woven Sylramic-iBN melt-infiltrated composites. *Compos Sci Technol* 2011, **71**: 52–59.

[16] Morscher GN, Pujar VV. Creep and stress–strain behavior after creep for SiC fiber reinforced, melt-infiltrated SiC matrix composites. *J Am Ceram Soc* 2006, **89**: 1652–1658.

[17] Wang H, Zhou X, Yu J, *et al*. Fabrication of $SiC_f$/SiC composites by chemical vapor infiltration and vapor silicon infiltration. *Mater Lett* 2010, **64**: 1691–1693.

[18] Morscher GN, Yun HM, DiCarlo JA. In-plane cracking behavior and ultimate strength for 2D woven and braided melt-infiltrated SiC/SiC composites tensile loaded in off-axis fiber directions. *J Am Ceram Soc* 2007, **90**: 3185–3193.

[19] Wang H, Zhou X, Yu J, *et al*. Microstructure, mechanical properties and reaction mechanism of KD-1 $SiC_f$/SiC composites fabricated by chemical vapor infiltration and vapor silicon infiltration. *Mat Sci Eng A* 2011, **528**: 2441–2445.

[20] Shimoda K, Park JS, Hinoki T, *et al*. Microstructural optimization of high-temperature SiC/SiC composites by NITE process. *J Nucl Mater* 2009, **386–388**: 634–638.

[21] Shimoda K, Hinoki T, Kishimoto H, *et al*. Enchanced high-temperature performances of SiC/SiC composites by high densification and crystalline structure. *Compos Sci Technol* 2011, **71**: 326–332.

[22] Park J-S, Kohyama A, Hinoki T, *et al*. Efforts on large scale production of NITE-SiC/SiC composites. *J Nucl Mater* 2007, **367–370**: 719–724.

[23] Yang B, Zhou X, Yu J. The properties of $C_f$/SiC composites prepared from different precursors. *Ceram Int* 2015, **41**: 4207–4213.

[24] Luo Z, Zhou X, Yu J, *et al*. Mechanical properties of SiC/SiC composites fabricated by PIP process with a new precursor polymer. *Ceram Int* 2014, **40**: 1939–1944.

[25] Bunsell AR, Piant A. A review of the development of three generations of small diameter silicon carbide fibres. *J Mater Sci* 2006, **41**: 823–839.

[26] Takeda M, Sakamoto J, Imai Y, *et al*. Thermal stability of the low-oxygen-content silicon carbide fiber Hi-Nicalon$^{TM}$. *Compos Sci Technol* 1999, **59**: 813–819.

[27] Katoh Y, Ozawa K, Shih C, *et al*. Continuous SiC fiber, CVI SiC matrix composites for nuclear applications: Properties and irradiation effects. *J Nucl Mater* 2014, **448**: 448–476.

[28] Yoshida K, Akimoto H, Yano T, *et al*. Mechanical properties of unidirectional and crossply $SiC_f$/SiC composites using SiC fibers with carbon interphase formed by electrophoretic deposition process. *Prog Nucl Energ* 2015, **82**: 148–152.

[29] Buet E, Sauder C, Sornin D, *et al*. Influence of surface fiber properties and textural organization of a pyrocarbon interphase on the interfacial shear stress of SiC/SiC minicomposites reinforced with Hi-Nicalon S and Tyranno SA3 fibres. *J Eur Ceram Soc* 2014, **34**: 179–188.

[30] Blagoeva DT, Hegeman JBJ, Jong M, *et al*. Characterisation of 2D and 3D Tyranno SA 3 CVI $SiC_f$/SiC composites. *Mat Sci Eng A* 2015, **638**: 305–313.

[31] Shimoda K, Hinoki T, Kohyama A. Effect of additive content on transient liquid phase sintering in SiC nanopowder infiltrated $SiC_f$/SiC composites. *Compos Sci Technol* 2011, **71**: 609–615.

[32] Abbé F, Chermant J-L. Fiber-matrix bond-strength characterization of silicon carbide-silicon carbide materials. *J Am Ceram Soc* 1990, **73**: 2573–2575.

[33] Wu H, Chen M, Wei X, *et al*. Deposition of BN interphase coatings from B-trichloroborazine and its effects on the mechanical properties of SiC/SiC composites. *Appl Surf Sci* 2010, **257**: 1276–1281.

[34] Ding D, Zhou W, Luo F, *et al*. Dip-coating of boron nitride interphase and its effects on mechanical properties of $SiC_f$/SiC composites. *Mat Sci Eng A* 2012, **543**: 1–5.

[35] Mu Y, Zhou W, Ding D, *et al*. Influence of dip-coated boron nitride interphase on mechanical and dielectric properties of $SiC_f$/SiC composites. *Mat Sci Eng A* 2013, **578**: 72–79.

[36] Lipp A, Schwetz KA, Hunold K. Hexagonal boron nitride: Fabrication, properties and applications. *J Eur Ceram Soc* 1989, **5**: 3–9.

[37] Sun N, Wang C, Jiao L, *et al*. Controllable coating of boron

nitride on ceramic fibers by CVD at low temperature. *Ceram Int* 2017, **43**: 1509–1516.

[38] Li J-S, Zhang C-R, Li B. Boron nitride coatings by chemical vapor deposition from borazine. *Surf Coat Technol* 2011, **205**: 3736–3741.

[39] Gao S, Li B, Zhang C, *et al*. Chemical vapor deposition of pyrolytic boron nitride ceramics from single source precursor. *Ceram Int* 2017, **43**: 10020–10025.

[40] Hu Y, Luo F, Duan S, *et al*. Mechanical and dielectric properties of $SiC_f$/SiC composites fabricated by PIP combined with CIP process. *Ceram Int* 2016, **42**: 6800–6806.

[41] Chai Y, Zhou X, Zhang H. Effect of oxidation treatment on KD–II SiC fiber–reinforced SiC composites. *Ceram Int* 2017, **43**: 9934–9940.

[42] Chai Y, Zhang H, Zhou X, *et al*. Effect of pyrolysis temperatures on the performance of $SiC_f$/SiC composites. *Fusion Eng Des* 2017, **125**: 447–453.

**Open Access** The articles published in this journal are distributed under the terms of the Creative Commons Attribution 4.0 International License (http://creativecommons.org/licenses/by/4.0/), which permits unrestricted use, distribution, and reproduction in any medium, provided you give appropriate credit to the original author(s) and the source, provide a link to the Creative Commons license, and indicate if changes were made.